Optik - International Journal for Light and Electron Optics xxx (xxxx) xxxx

Contents lists available at ScienceDirect

Optik

journal homepage: www.elsevier.com/locate/ijleo

Original research article

Precision of kinematic coupling mechanism for optical instruments

Ye Yuan[a,b,*], Liheng Chen[a], Libao Yang[a], Jihong Dong[a], Shuyan Xu[a], Shuxin Wang[a]

[a] Changchun Institute of Optics, Fine Mechanics and Physics, Chinese Academy of Sciences, Changchun 130033, China
[b] University of Chinese Academy of Sciences, Beijing 100049, China

ARTICLE INFO

Keywords:
Kinematic coupling
Optical instrument
Precision
Deformation
Displacement

ABSTRACT

This paper designs a kinematic coupling mechanism to enable the stress-free connection between the mounting platform and the optical instrument. Firstly, the author theoretically analyzed how the mechanism deformation affects the position of the instrument center, aiming to identify the exact relationship between instrument precision, coupling layout and coupling displacement. Next, the relationship between mechanism deformation and the center position was computed by homogenous transformation matrices, yielding the analytical solution to the center position, coupling layout and coupling displacement. The research findings shed new light on the free-stress coupling and precision improvement of optical instruments.

1. Introduction

Remote sensors are increasing in size and mass to achieve better resolution of space observation. Once a remote sensor is in orbit, factors like gravity release and thermal deformation will cause a huge stress between the optical system and the coupling structure. The mirror will be distorted under the stress, reducing the imaging quality of the optical system. This problem can be generally solved using flexible coupling and strict control of temperature.

In the James Webb Space Telescope (JWST) [1–4], both the Integrated Science Instrument Module (ISIM) and the Fine Guidance Sensor (FGS) [5,6] are connected to the main structure via quasi-kinematic coupling, which restrain the transfer of mechanical and thermal deformations between the ISIM and the main structure. The Hexapod coupling [7–20] is adopted to prop up the main structure of Large Synoptic Survey Telescope (LSST), DGT telescope, Subaru telescope, and Large Binocular Telescope (LBT), and the secondary mirror of the Multiple Mirror Telescope (MMT) [21–25].

During on-orbit replacement, there is a large difference in temperature between the optical system and the mounting platform, as well as in the size of mounting interface between different instruments. The temperature and size differences may induce stress on the optical system. This calls for novel methods to minimize the differences and eliminate the stress.

Based on the theory of constraints, this paper develops a kinematic coupling mechanism to ensure that no object is over- or under-constrained. As a statically determinant structure, the proposed mechanism can eliminate the stress between the optical system and the mounting platform, which may arise from the said temperature and size differences. In addition, the coupling mechanism boasts a high precision, and has little impact on the imaging quality of the optical system.

2. Design of kinematic coupling

Focusing on operability, this paper designs a kinematic coupling mechanism consisting of a sphere in a tapered groove, a sphere in

* Corresponding author.
E-mail address: yuanye080888@163.com (Y. Ye).

https://doi.org/10.1016/j.ijleo.2019.163592
Received 20 July 2019; Accepted 11 October 2019

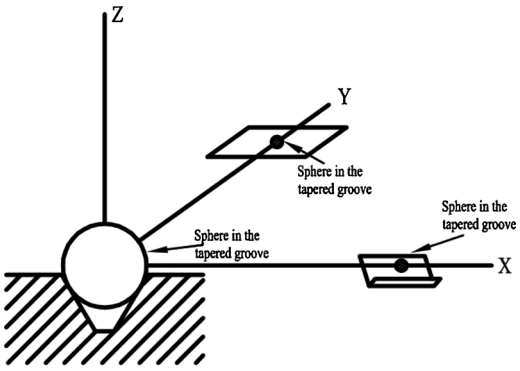

Fig. 1. The schematic diagram of the proposed coupling mechanism.

a v-groove and a sphere on a plane. The schematic diagram of the proposed coupling mechanism is presented as Fig. 1. The optical instrument must press against the coupling. Normally, this can be achieved due to the gravity of the instrument. When there is no gravity, springs should be added to ensure complete contact between the instrument and the coupling.

As shown in Fig. 1, the tapered groove constrains the translation of the sphere centering at point A in the x, y and z directions; the v-groove constraints the translation of the sphere centering at point B in the y and z directions; the two grooves jointly constrain the rotation of the spheres about the y- axis and the z-axis, while allowing the rotation about the x-axis; the plane constrains the motion of the sphere centering at point C perpendicular to the x–y plane, i.e. the rotation about the x-axis. To sum up, the tapered groove, the v-groove and the plane respectively constrain 3, 2 and 1 degrees-of-freedom (DOFs) of the spheres. Thus, the coupling form is called the "3-2-1" pattern.

The rotation and translation of the spheres can eliminate the deformations induced by the gravity release, stress and heat, after an optical instrument has entered the orbit. In this way, all the connections become stress-free, thus ensuring the imaging quality of the optical instrument.

3. Kinematic model analysis

To achieve stress-free coupling, the kinematic mechanism needs to make adjustment automatically depending on the specific size of the structure. The adjustment will lead to changes in the mounting position of the optical instrument. Any disordered, unknown or uncontrollable change will undermine the imaging quality. In this paper, the three sphere centers are connected into a triangle, and the triangular center is selected to represent the instrument position. Based on the displacements of the three sphere centers, the variation law of the triangular center coordinates was solved to reveal the positioning and direction precisions of the instrument.

As shown in Fig. 2, points A, B and C are the three sphere centers before the deformation of the optical instrument, while points A, B1 and C1 are the three sphere centers after the deformation. The angle between the line AB and the motion direction of point B (x axis) is defined as the distribution angle α. Taking point A as the origin, a Cartesian coordinate system was established with the motion direction of point B as the x axis. Then, the coordinates of the sphere centers before and after the deformation can be expressed by homogenous transformation matrices.

The coordinates of point B can be expressed as:

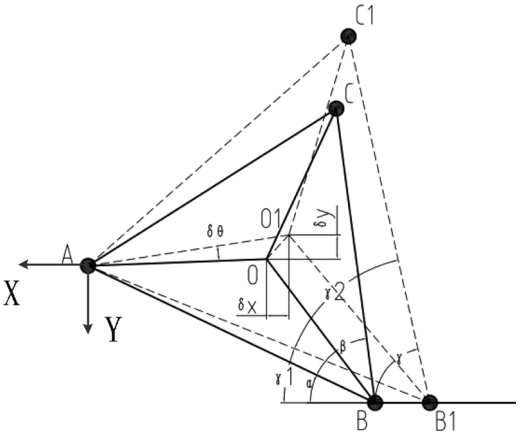

Fig. 2. Geometric model of the kinetic mechanism.

$$\begin{bmatrix} X_B \\ Y_B \\ Z_B \\ 1 \end{bmatrix} = T_{lz}(-\alpha)T_x(-L_{AB})\begin{bmatrix} 0 \\ 0 \\ 0 \\ 1 \end{bmatrix} \tag{1}$$

The coordinates of point C can be expressed as:

$$\begin{bmatrix} X_C \\ Y_C \\ Z_C \\ 1 \end{bmatrix} = T_{lz}(-\beta)T_x(L_{BC})\begin{bmatrix} X_B \\ Y_B \\ Z_B \\ 1 \end{bmatrix} \tag{2}$$

The coordinates of point B1 can be expressed as:

$$\begin{bmatrix} X_{B_1} \\ Y_{B_1} \\ Z_{B_1} \\ 1 \end{bmatrix} = T_{lz}(-\alpha)T_x(-L_{AB})T_{lz}(\alpha)T_x(-L_{BB_1})\begin{bmatrix} 0 \\ 0 \\ 0 \\ 1 \end{bmatrix} \tag{3}$$

The coordinates of point C1 can be expressed as:

$$\begin{bmatrix} X_{C_1} \\ Y_{C_1} \\ Z_{C_1} \\ 1 \end{bmatrix} = T_{lz}(-\alpha)T_x(-L_{AB})T_{lz}(\alpha)T_x(-L_{BB_1})T_{lz}(-\gamma)T_x(L_{B_1C_1})\begin{bmatrix} 0 \\ 0 \\ 0 \\ 1 \end{bmatrix} \tag{4}$$

where $T_{lz}(\theta)$ can be described as:

$$T_{lz}(\theta) = \begin{bmatrix} \cos\theta & -sin\theta & 0 & 0 \\ sin\theta & \cos\theta & 0 & 0 \\ 0 & 0 & 1 & 0 \\ 0 & 0 & 0 & 1 \end{bmatrix} \tag{5}$$

And $T_X(\mathrm{P})$ can be described as:

$$T_X(\mathrm{P}) = \begin{bmatrix} 1 & 0 & 0 & P \\ 0 & 1 & 0 & 0 \\ 0 & 0 & 1 & 0 \\ 0 & 0 & 0 & 1 \end{bmatrix} \tag{6}$$

Substituting (5) and (6) into (1)~(4), the coordinates of points B, C, B1 and C1 can be obtained as:

$$\begin{bmatrix} X_B \\ Y_B \end{bmatrix} = \begin{bmatrix} -L_{AB}cos\alpha \\ L_{AB}sin\alpha \end{bmatrix} \tag{7}$$

$$\begin{bmatrix} X_C \\ Y_C \end{bmatrix} = \begin{bmatrix} -L_{AC}\cos(\beta-\alpha) \\ -L_{AC}\sin(\beta-\alpha) \end{bmatrix} \tag{8}$$

$$\begin{bmatrix} X_{B_1} \\ Y_{B_1} \end{bmatrix} = \begin{bmatrix} -L_{AB}cos\alpha - L_{BB_1} \\ L_{AB}sin\alpha \end{bmatrix} \tag{9}$$

$$\begin{bmatrix} X_{C_1} \\ Y_{C_1} \end{bmatrix} = \begin{bmatrix} -L_{AB}\cos\alpha + L_{B_1C_1}cos\,\gamma - L_{BB_1} \\ L_{AB}\sin\alpha - L_{B_1C_1}sin\gamma \end{bmatrix} \tag{10}$$

The coordinates of the triangular center before deformation can be expressed as:

$$\begin{bmatrix} X_o \\ Y_o \\ Z_o \end{bmatrix} = \frac{1}{3}\left(\begin{bmatrix} X_A \\ Y_A \\ Z_A \end{bmatrix} + \begin{bmatrix} X_B \\ Y_B \\ Z_B \end{bmatrix} + \begin{bmatrix} X_C \\ Y_C \\ Z_C \end{bmatrix}\right) \tag{11}$$

Substituting (7) and (8) into (11), the coordinates of point O can be obtained as:

$$\begin{bmatrix} X_o \\ Y_o \end{bmatrix} = \frac{1}{3}\begin{bmatrix} -L_{AB}\cos\alpha - L_{AC}\cos(\beta-\alpha) \\ -L_{AC}\sin(\beta-\alpha) + L_{AB}sin\alpha \end{bmatrix} \tag{12}$$

The coordinates of the triangular center after deformation can be expressed as:

$$\begin{bmatrix} X_{O_1} \\ Y_{O_1} \\ Z_{O_1} \end{bmatrix} = \frac{1}{3}\left(\begin{bmatrix} X_A \\ Y_A \\ Z_A \end{bmatrix} + \begin{bmatrix} X_{B_1} \\ Y_{B_1} \\ Z_{B_1} \end{bmatrix} + \begin{bmatrix} X_{C_1} \\ Y_{C_1} \\ Z_{C_1} \end{bmatrix} \right) \tag{13}$$

Substituting (9) and (10) into (13), the coordinates of point O_1 can be obtained as:

$$\begin{bmatrix} X_{o_1} \\ Y_{o_1} \end{bmatrix} = \frac{1}{3}\begin{bmatrix} -2L_{AB}cos\alpha - 2L_{BB_1} + L_{B_1C_1}cos\gamma \\ 2L_{AB}sin\alpha - L_{B_1C_1}sin\gamma \end{bmatrix} \tag{14}$$

The positioning precision of the optical instrument can be illustrated by the change of triangular center coordinates through the deformation δ_x and δ_y:

$$\begin{bmatrix} \delta_x \\ \delta_y \end{bmatrix} = \begin{bmatrix} X_{O_1} - X_O \\ Y_{O_1} - Y_O \end{bmatrix} \tag{15}$$

Substituting (12) and (14) into (15), δ_x and δ_y can be calculated as:

$$\begin{bmatrix} \delta_x \\ \delta_y \end{bmatrix} = \frac{1}{3}\begin{bmatrix} -2L_{BB_1} - L_{AB}\cos\alpha + L_{B_1C_1}cos\gamma + L_{AC}\cos(\beta-\alpha) \\ L_{AB}sin\alpha - L_{B_1C_1}sin\gamma + L_{AC}\sin(\beta-\alpha) \end{bmatrix} \tag{16}$$

4. Error analysis

This section aims to disclose how key model parameters like distribution angle α and temperature variation ΔT affect error variation. To reduce the number of unknown terms, it is assumed that the sphere centers are the vertices of a regular triangle and have the same displacement, that is, the triangle remains regular through the deformation.

4.1. Trajectory of triangular center

The parameters in (16) can be determined by the cosine law, based on the side length of the triangle L_{AB}, the relative change of the length $\mu\Delta T$ and the distribution angle α. Thus, the formula of δ_x and δ_y can be simplified as:

$$\delta_y = \frac{1}{3}L_{AB}\left(\cos\left(\alpha+\frac{\pi}{6}\right) + s\ in\alpha - (1+\mu\Delta T)\sin\theta\right) \tag{17}$$

$$\delta_x = \frac{\sqrt{3}}{3}L_{AB}\left(\cos\left(\alpha+\frac{\pi}{6}\right) + s\ in\alpha - (1+\mu\Delta T)\sin\theta\right) \tag{18}$$

where

$$\theta = \frac{\pi}{6} + \mathrm{ArcCsc}\left(\frac{1+\mu\Delta T}{\sqrt{\mu\Delta T(2+\mu\Delta T) + cos^2\alpha}}\right) \tag{19}$$

From (17) and (18), the relationship between δ_x and δ_y can be determined as:

$$\delta_y = \sqrt{3}\delta_x \tag{20}$$

As shown in (20), δ_x and δ_y maintain a fixed proportional relationship, which is independent of other parameters. This means, however the coupling size changes, the instrument center will still move along a linear path, starting from the original center. The trajectory will deviate from the motion direction of point B by 30°. The motion trajectory of the instrument center is presented in Fig. 3 below.

4.2. Factors affects the displacement variation of instrument center

For the optical instrument, the displacement variation of its center is negatively correlated with stability. The distribution angle and temperature variation are the leading impactors of the displacement variation of the instrument center. To optimize the coupling design, it is highly necessary to disclose the influence mechanism of the two factors on the displacement variation. The law of the relative displacement of the instrument center ($\frac{\delta_y}{L_{AB}}$) can be derived from (17) and (18) as:

$$\frac{\delta_y}{L_{AB}} = \frac{1}{3}\left(\cos\left(\alpha+\frac{\pi}{6}\right) + s\ in\alpha - (1+\mu\Delta T)\sin\theta\right) \tag{21}$$

where

$$\theta = \frac{\pi}{6} + \mathrm{ArcCsc}\left(\frac{1+\mu\Delta T}{\sqrt{\mu\Delta T(2+\mu\Delta T) + cos^2\alpha}}\right) \tag{22}$$

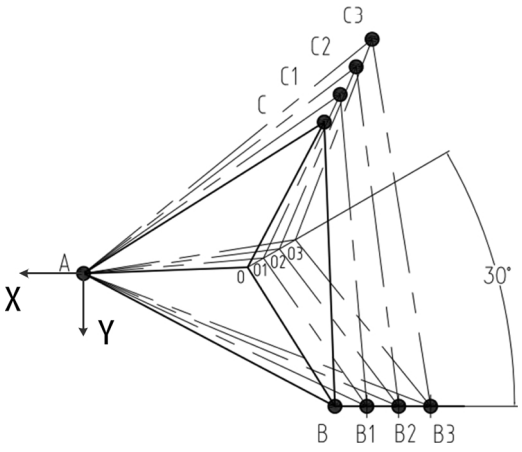

Fig. 3. The motion trajectory of the instrument center.

The correlation of the relative displacement of the instrument center with distribution angle and temperature variation was plotted on Matlab (μ = 9e-6), and displayed as Fig. 4 below.

(1) Effect of distribution angle

It can be seen from Fig. 4 that the relative displacement of the instrument center increases with the distribution angle. To reveal the exact influence mechanism, it is assumed that relative change of the side length of the triangle $\mu\Delta T$ remains constant ($\mu\Delta T$ = 3.6e-4). On this basis, the relative displacement of the instrument center was solved at each distribution angle on Matlab. The relationship between the two parameters is shown in Fig. 5 below.

As shown in Fig. 5, the relative displacement of the instrument center exhibits a nonlinear growth with the increase of the distribution angle. The relative displacement reaches the minimum at α= 0°, grows slightly when α<20°, and increases at a much faster rate when α>40°.

(2) Effect of temperature variation

It can also be seen from Fig. 4 that the relative displacement of the instrument center increases with the temperature variation. To reveal the exact influence mechanism, it is assumed that the distribution angle α remains constant (α = 0). The partial derivative of ΔT can be obtained from (23) as:

$$\frac{\partial(\frac{\delta_y}{L_{AB}})}{\partial(\Delta T)} = -\frac{1}{3}\mu\sin\left(\frac{2\pi}{3}-\alpha\right) \tag{23}$$

The above formula indicates that the relative displacement of the instrument center is linearly correlated with temperature variation when the value of α remains constant. Then, the relative displacement of the instrument center was solved under different temperature variations on Matlab. The relationship between the two parameters is shown in Fig. 6 below.

As shown in Fig. 5, the relative displacement of the instrument center exhibits a nonlinear growth with the increase of the temperature variation.

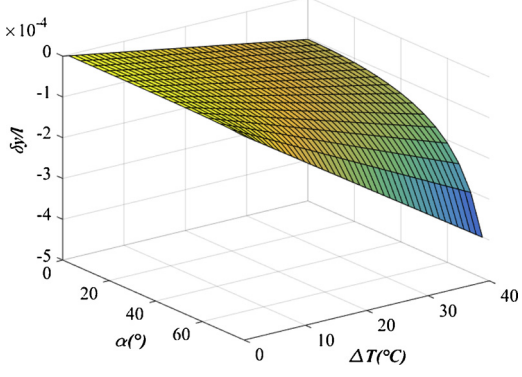

Fig. 4. Trend of the relative displacement of the instrument center.

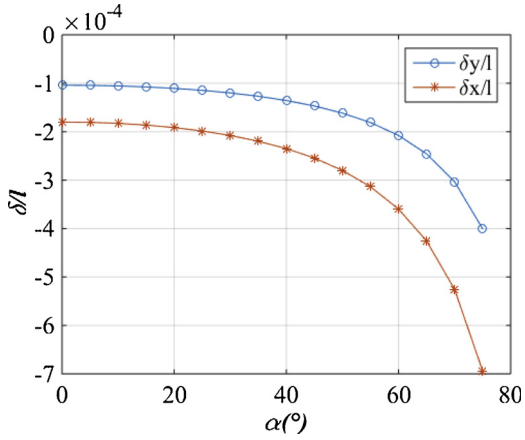

Fig. 5. Effect of distribution angle on the relative displacement of the instrument center.

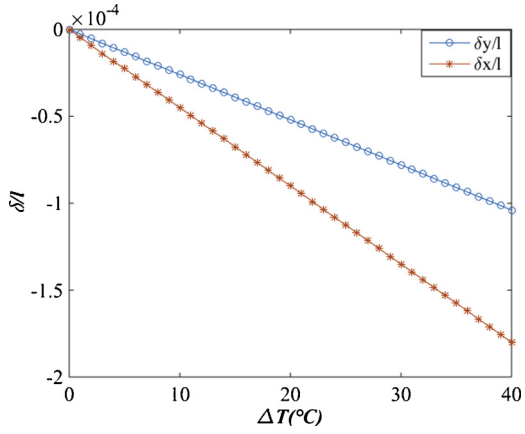

Fig. 6. Effect of temperature variation on the relative displacement of the instrument center.

5. Conclusions

This paper designs a kinematic coupling mechanism to enable the stress-free connection between the mounting platform and the optical instrument. Firstly, the kinematic model of the mechanism was analyzed theoretically, yielding the analytical expressions for the instrument center, the three couplings, and their displacements. Based on these expressions, the author summed up the variation laws of the positioning and direction precisions of the coupling mechanism. The calculation results show that the instrument center can move stably along a straight line, when the three couplings form a regular triangle. In addition, the relative displacement of the instrument center can surpass 0.02% in stability in the two mutually perpendicular directions, when the coupling mechanism undergoes a temperature variation of over 40 °C. These laws shed important light on the optimal design of similar kinematic coupling mechanisms, and provide a valuable reference for rationalizing the service environment, manufacture precision and compensation control of optical instruments.

Acknowledgement

The author(s) disclosed receipt of the following financial support for the research and/or authorship of this article:
This work is supported by the National Natural Science Foundation of China (NO. 11873046).

References

[1] M.A. Greenhouse, P.C. Sullivan, L.A. Boyce, S.D. Glazer, E.L. Johnson, J.C. McCloskey, M.F. Voyton, The James Webb Space Telescope integrated science instrument module, Proc. SPIE (2004) 754–764 5487.
[2] Brent J. Bos, Joseph M. Howard, Philip J. Young, Renee Gracey, Lenward T. Seals, Raymond G. Ohl, "Global alignment optimization strategies, procedures, and tools for the James Webb Space Telescope (JWST) Integrated Science Instrument Module (ISIM)", Proc. SPIE 8442, Space Telescopes and Instrumentation 2012: Optical, Infrared, and Millimeter Wave, 84423I (2012/09/21).
[3] G.S. Wright, et al., The JWST MIRI instrument concept, Proc. SPIE (2004) 653–663 5487.
[4] N. Rowlands, et al., The JWST fine guidance sensor, Proc. SPIE (2004) 664–675 5487.

[5] N. Rowlands, C. Evans, E. Greenberg, P. Gregory, A. Scott, S. Thibault, M. Poirer, R. Doyon, J. Hutchings, R. Alexander, Tunable filters for JWST Fine Guidance Sensor, Proc. SPIE (2004) 676–687 5487.
[6] B.J. Bos, D.A. Kubalak, S.R. Antonille, R.G. Ohl, J.G. Hagopian, P.S. Davila, J. Sullivan, M. Sánchez, Cryogenic pupil alignment test architecture for the James Webb Space Telescope integrated science instrument module, Proc. SPIE (2008) 70103C 7010.
[7] D. Neill, E. Hileman, J. Sebag, W. Gressler, O. Wiecha, M. Warner, J. Andrew, B. Schoening, Baseline design of the LSST Telescope Mount assembly, Proc. SPIE (2014) 9145.
[8] D. Neill, W. Gressler, J. Sebag, O. Wiecha, M. Warner, B. Schoening, J. DeVries, J. Andrew, G. Schumacher, E. Hileman, LSST secondary mirror assembly baseline design, Proc. SPIE (2012) 9444.
[9] D. Neill, E. Hileman, LSST Telescope primary/tertiary mirror cell assembly, Proc. SPIE (2010) 7733.
[10] D. Neill, G. Angeli, C. Claver, E. Hileman, J. DeVries, S. Sebag, B. Xin, Overview of the LSST active optics system, Proc. SPIE (2014) 9150.
[11] D. Neill, Seismic analysis of the LSST telescope, Proc. SPIE (2012) 8444.
[12] D. Neill, M. Warner, J. Sebag, Seismic design accelerations for the LSST, Proc. SPIE (2012) 8444.
[13] Schmidt-Kaler, The Hexapod telescope, a new way to very large telescopes, in: M.H. Ulrich (Ed.), Progress in Telescope and Instrumentation Technologies, 117 ESO, Munich, 1992.
[14] Rolf Chini, The Hexapod telescope, a never-ending story, in: R.E. Schielicke (Ed.), Reviews in Modern Astronomy 13: New Astrophysical Horizons, Astronomische Gesellschaft, Hamburg, Germany, 2000p. 257.
[15] Philippe A. Raffin, Robert N. Martin, Yau-De Huang, Ferdinand Patt, Robert C. Romeo, Ming-Tang Chen, Jeffrey S. Kingsley, "CFRP platform and hexapod mount for the Array of Microwave Background Anisotropy," Proc. SPIE Vol. 5495, p. 159-167, Astronomical Structures and Mechanisms Technology, Joseph Antebi, Dietrich Lemke, eds., 2004. Proc. of SPIE Vol. 6273 62731F-16.
[16] Miyawaki, et al., Mechanical structure of the SUBARU telescope, in: L.D. Barr (Ed.), Proc SPIE Conf. on Advanced Technology Optical Telescopes V, 1994, pp. 754–764 2199.
[17] Conrad Neufeld, Victor Bennett, Andrea Sarnik, Gregory Ruthven, Keane Michael, Thomas A. Sebring, Victor L. Krabbendam, Development of an active optical system for the SOAR telescope, Proc. SPIE (2004) 1052–1060 5489.
[18] C. Pernechele, F. Bortoletto, K. Reif, Hexapod control for an active secondary mirror: general concept and test results, Appl. Opt. 37 (1998) 6816–6821.
[19] Daniele Gallieni, et al., LBT adaptive secondary units final design and construction, Adaptive Optical System Technologies II. Edited by Wizinowich, Peter L.; Bonaccini, Domenico, Proc. SPIE (2003) 765–771 4839.
[20] P.M. Gray, S.C. West, W. Gallieni, Support and actuation of six secondaries for the 6.5 m MMT and 8.4 m LBT telescopes, Proc. SPIE Conf. on Optical Telescopes of Today and Tomorrow (1996) 2871.
[21] Michael Lloyd-Hart, et al., Adaptive optics for the 6.5-m MMT, in: Peter L. Wizinowich (Ed.), Proc. SPIE Vol. 4007, pp. 167–174, Adaptive Optical Systems Technology, 2000.
[22] Enrique Garcia, Lorenzo Zago, Daniele Gallieni, Special and innovative aspects of the GTC M2 drive mechanism, Large Ground-Based Telescopes. Edited by Oschmann, Jacobus M.; Stepp, Larry M. Proc. SPIE (2003) 448–455 4837.
[23] Matthew W. Johns, Giant Magellan Telescope, Emerging Optoelectronic Applications. Edited by Jabbour, Ghassan E.; Rantala, Juha T. Proc. SPIE (2004) 85–94 5382.
[24] Eric H. Anderson, John P. Fumo, R. Scott Erwin, Satellite ultraquiet isolation technology experiment, IEEE Aerospace Conference, Big Sky, MO (2000).
[25] Jonathan L. Hall, Gregory W. Pettit, Jason E. Lindler, Eric H. Anderson, Eric M. Flint, Compact lightweight six-axis point-and-hold positioning system, SPIE Smart Structures Symposium: Industrial and Commercial Apps. Of Smart Structures Technologies, San Diego, Mar, 2003 SPIE 5054-33.